



CrossMark

Formation of All Three C₂H₄O Isomers—Ethylene Oxide (*c*-C₂H₄O), Acetaldehyde (CH₃CHO), and Vinyl Alcohol (CH₂CHOH)—in Ethanol-containing Interstellar Analog Ices

Jia Wang^{1,2} , Chaojiang Zhang^{1,2} , Joshua H. Marks^{1,2} , and Ralf I. Kaiser^{1,2} ¹ W. M. Keck Research Laboratory in Astrochemistry, University of Hawaii at Manoa, Honolulu, HI 96822, USA; ralfk@hawaii.edu² Department of Chemistry, University of Hawaii at Manoa, Honolulu, HI 96822, USA

Received 2025 January 16; revised 2025 March 17; accepted 2025 March 18; published 2025 May 6

Abstract

Oxygen-containing complex organic molecules are key precursors to biorelevant compounds fundamental for the origins of life. However, the untangling of their interstellar formation mechanisms has just scratched the surface, especially for oxygen-containing cyclic molecules. Here, we present the first laboratory simulation experiments featuring the formation of all three C₂H₄O isomers—ethylene oxide (*c*-C₂H₄O), acetaldehyde (CH₃CHO), and vinyl alcohol (CH₂CHOH)—in low-temperature model interstellar ices composed of carbon monoxide (CO) and ethanol (C₂H₅OH). Ice mixtures were exposed to galactic cosmic-ray proxies with an irradiation dose equivalent to a cold molecular cloud aged $(7 \pm 2) \times 10^5$ yr. These biorelevant species were detected in the gas phase through isomer-selective photoionization reflectron time-of-flight mass spectrometry during temperature-programmed desorption. Isotopic labeling experiments reveal that ethylene oxide is produced from ethanol alone, providing the first experimental evidence to support the hypothesis that ethanol serves as a precursor to the prototype epoxide in interstellar ices. These findings reveal feasible pathways for the formation of all three C₂H₄O isomers in ethanol-rich interstellar ices, offering valuable constraints on astrochemical models for their formation. Our results suggest that ethanol is a critical precursor to C₂H₄O isomers in interstellar environments, representing a critical step toward unraveling the formation mechanisms of oxygen-containing cyclic molecules, aldehydes, and their enol tautomers from alcohols in interstellar ices.

Unified Astronomy Thesaurus concepts: Laboratory astrophysics (2004); Astrochemistry (75); Mass spectrometry (2094); Complex organic molecules (2256); Interstellar molecules (849)

1. Introduction

Since the first detection of methanol (CH₃OH) in the interstellar medium (ISM) by J. A. Ball et al. (1970) toward Sagittarius A and the Sagittarius B2 (Sgr B2) molecular cloud complex more than half a century ago (J. A. Ball et al. 1970), oxygen-containing complex organic molecules (COMs)—organic molecules containing six or more atoms (E. Herbst & E. F. V. Dishoeck 2009)—have garnered extensive attention from the laboratory astrophysics (J. M. Bernard et al. 2003; C. J. Bennett et al. 2005b; D. Skouteris et al. 2018; K. M. Yocum et al. 2021), astrochemistry (M. J. Abplanalp et al. 2016; N. F. Kleimeier et al. 2021b; B. Bhat et al. 2023), physical organic chemistry (Z. Dai et al. 2014; H. S. P. Müller et al. 2023b), and theoretical chemistry (A. Occhiogrosso et al. 2012; A. Karton & D. Talbi 2014; V. Barone et al. 2015) communities. To date, 39 oxygen-containing COMs have been identified in the ISM, accounting for 11% of the 349 known interstellar molecules (D. E. Woon 2025). These molecules represent key organic classes, including alcohols (–OH), aldehydes (–CHO), ketones (–CO–), carboxylic acids (–COOH), esters (–COO–), amides (–CONH–), and epoxides (–[*c*-CHOCH]–). Oxygen-containing COMs are not only considered key tracers of nonequilibrium chemistry in interstellar icy grains (N. F. Kleimeier et al. 2021a; H. M. Cuppen et al. 2024) but also play a critical role in the synthesis of

biorelevant molecules fundamental for the origins of life (C. Puzzarini et al. 2017; M. K. Sharma et al. 2018; J. Wang et al. 2024a).

Among the oxygen-containing COMs detected in circumstellar and interstellar environments, only two oxygen-containing cyclic molecules have been identified. Ethylene oxide (oxirane; *c*-C₂H₄O) belongs to the C₂H₄O family (Figure 1(a)) and has been detected toward Sagittarius B2N (Sgr B2N; J. E. Dickens et al. 1997), the solar-type protostar IRAS 16293–2422 (H. S. P. Müller et al. 2023a), and the star-forming regions NGC 6334F, G327.3–0.6, and G31.41+0.31, with fractional abundances reaching 6×10^{-10} relative to molecular hydrogen (H₂) (A. Nummelin et al. 1998). Notably, the two other stable C₂H₄O isomers, acetaldehyde (CH₃CHO) and vinyl alcohol (CH₂CHOH), have also been identified in the ISM. Acetaldehyde has been identified toward star-forming regions such as Orion-KL (B. E. Turner 1991; L. M. Ziurys & D. McGonagle 1993; S. B. Charnley 2004), NGC 6334F, G327.3–0.6, and G31.41+0.31 (A. Nummelin et al. 1998; M. Ikeda et al. 2001), Sgr B2 (N. Fourikis et al. 1974; M. B. Bell et al. 1983), molecular clouds like Taurus molecular cloud (TMC-1) & L134N (H. E. Matthews et al. 1985), and the translucent object CB 17 (B. Turner et al. 1999). Additionally, acetaldehyde has been tentatively detected in interstellar ices (E. L. Gibb et al. 2004; M. K. McClure et al. 2023; W. R. M. Rocha et al. 2024) toward protostar W33A at levels of a few percent relative to water (H₂O; E. L. Gibb et al. 2004). Vinyl alcohol, the simplest enol, has been detected toward Sgr B2N with a column density of 2.2×10^{14} cm^{–2} (B. E. Turner & A. J. Apponi 2001). Through nonequilibrium chemistry



Original content from this work may be used under the terms of the [Creative Commons Attribution 4.0 licence](https://creativecommons.org/licenses/by/4.0/). Any further distribution of this work must maintain attribution to the author(s) and the title of the work, journal citation and DOI.

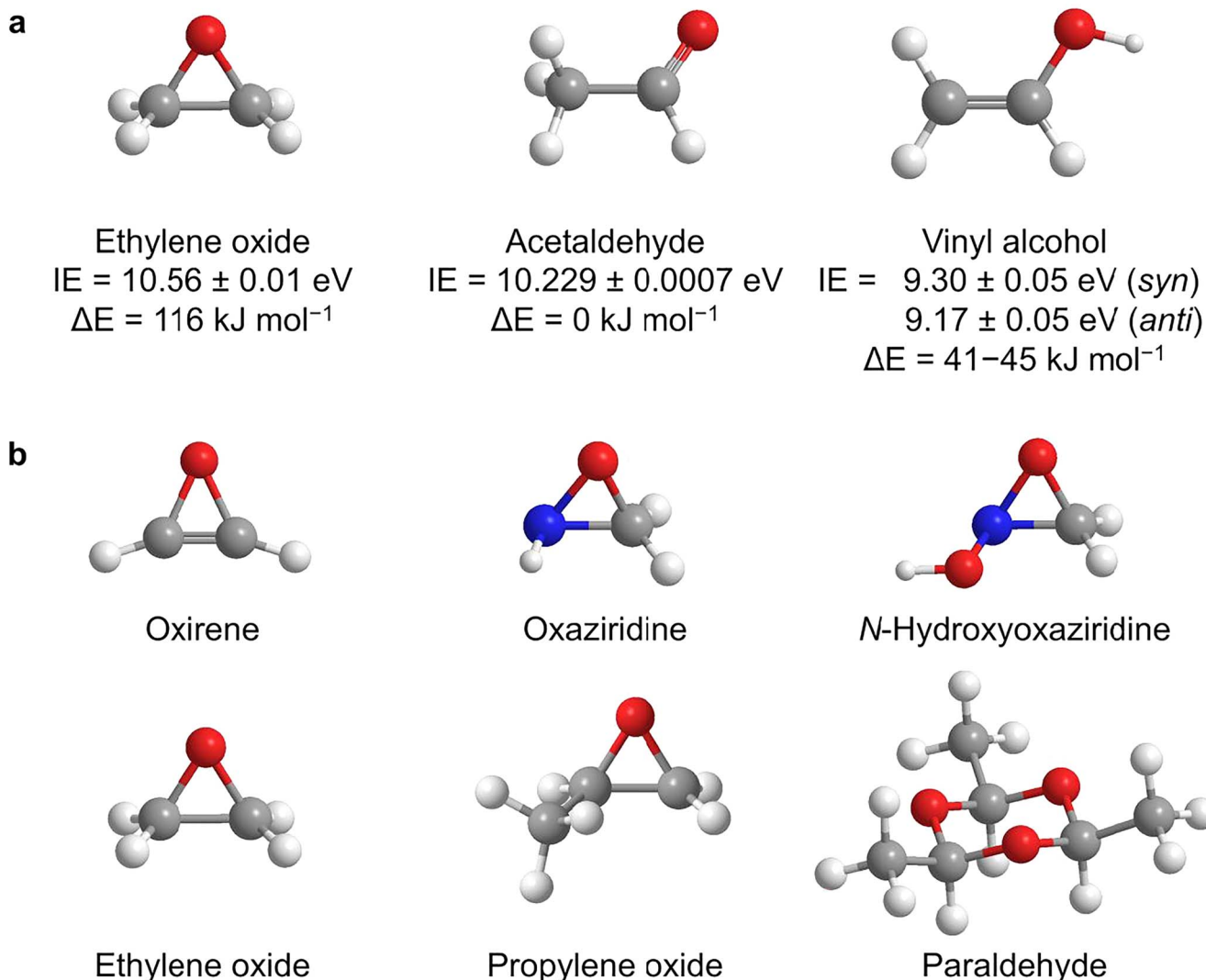


Figure 1. (a) C₂H₄O isomers with experimental adiabatic ionization energies (IEs) (G. Y. Matti et al. 1989; S. G. Lias 2024) and computed relative energies (ΔE ; M.-A. Martin-Drumel et al. 2019). (b) Oxygen-containing ring molecules identified in interstellar analog ices.

driven by ionizing radiation, these C₂H₄O isomers serve as key precursors to biorelevant COMs such as amino acids (N. F. Kleimeier et al. 2020a; N. F. Kleimeier et al. 2020b), chelating agents (J. H. Marks et al. 2023), and sugar derivatives (J. Wang et al. 2024a). In addition to ethylene oxide, the chiral molecule propylene oxide (*c*-C₃H₆O) has been identified toward Sgr B2N with a column density of 1×10^{13} cm⁻² and a rotational excitation temperature of 5 K (B. A. McGuire et al. 2016). The identification of propylene oxide offers possibilities to unravel the chemical and physical processes that may explain the origin of chirality in the Universe (A. Bergantini et al. 2018a; S. Thripati et al. 2023).

Laboratory simulation experiments have revealed the formation of oxygen-containing cyclic molecules in processed interstellar analog ices (Figure 1(b)). Oxirene (*c*-C₂H₂O)—a prototype of highly strained antiaromatic organics—was prepared in low-temperature acetaldehyde–methanol (CH₃CHO–CH₃OH) ice exposed to energetic electrons at 5 K and stabilized through resonant energy transfer prior to gas-phase detection (J. Wang et al. 2023a). Oxaziridine (*c*-H₂CONH) and *N*-hydroxyoxaziridine (*c*-H₂CON(OH)) were formed in electron-irradiated methane–nitrogen monoxide

(CH₄–NO) ice (S. K. Singh et al. 2020a) and methane–nitrogen dioxide (CH₄–NO₂) ice (S. K. Singh et al. 2020b) via the addition of carbene ($\dot{\text{C}}\text{H}_2$) to the nitrogen-oxygen double bond of nitrosyl hydride (HNO) and nitrous acid (HONO), respectively. Through the addition of a suprathreshold oxygen atom to the carbon–carbon double bond of an ethylene (C₂H₄) molecule, ethylene oxide was formed from carbon dioxide–ethylene (CO₂–C₂H₄) ice via electron irradiation (C. J. Bennett et al. 2005b) and vacuum ultraviolet (VUV) photolysis (J. B. Bergner et al. 2019). Additionally, surface reactions of isolated ground-state oxygen atoms (O(³P)) with ethylene at temperatures ranging from 12 to 90 K may have resulted in the formation of ethylene oxide as the major product (M. D. Ward & S. D. Price 2011). Propylene oxide was synthesized via cosmic-ray-mediated reactions in low-temperature carbon dioxide–propylene (CO₂–C₃H₆) ice (A. Bergantini et al. 2018a) and methane–acetaldehyde (CH₄–CH₃CHO) ice (S. K. Singh et al. 2022). Recently, the cyclic acetaldehyde trimer, paraldehyde (*c*-C₆H₁₂O₃), was prepared via polymerization in low-temperature acetaldehyde ices exposed to electron irradiation (J. Wang et al. 2024c). These findings suggest that oxygen-containing cyclic molecules can be

ubiquitous in star-forming regions and act as energetic precursors for the abiotic formation of other COMs in the interstellar environment. Despite the laboratory simulation efforts, the interstellar formation mechanisms of oxygen-containing cyclic molecules have remained poorly understood; even for relatively simple ones such as ethylene oxide and propylene oxide, a comprehensive understanding of their formation pathways remains incomplete. It has been suggested that ethanol can serve as a precursor to the interstellar ethylene oxide (M. Ikeda et al. 2001; A. Occhiogrosso et al. 2012; D. Skouteris et al. 2018); however, experimental evidence to support this hypothesis is still lacking.

Here, we present the first laboratory experiments on the formation of all three C_2H_4O isomers—ethylene oxide (*c*- C_2H_4O), acetaldehyde (CH_3CHO), and vinyl alcohol (CH_2CHOH)—which occurs in low-temperature model interstellar ices composed of carbon monoxide and ethanol ($CO-CH_3CH_2OH$). Carbon monoxide has been identified as a major component of interstellar ices, with an abundance of up to 55% relative to water toward IRAS 08375–4109 (W.-F. Thi et al. 2006). Ethanol has been tentatively detected in ices toward background stars such as NIR38 and J110621 (M. K. McClure et al. 2023) and young protostars such as IRAS 2A and IRAS 23385, with abundances reaching up to 1.8% relative to water (W. R. M. Rocha et al. 2024). Additionally, laboratory experiments have revealed that ethanol can be formed from readily available precursors such as water, methanol, and methane in interstellar ices (A. Bergantini et al. 2017; A. Bergantini et al. 2018b). The mixed ices were irradiated at a temperature of 5 K with energetic electrons, which simulate the secondary electrons released as galactic cosmic-ray (GCR) transit clouds, to produce irradiation doses equivalent to $(7 \pm 2) \times 10^5$ yr of GCR exposure in a cold molecular cloud (A. G. Yeghikyan 2011). Utilizing VUV photoionization reflectron time-of-flight mass spectrometry (PI-ReToF-MS) and isotopic substitution experiments, all three C_2H_4O isomers were detected in the gas phase during temperature-programmed desorption (TPD) on the basis of their adiabatic ionization energies (IEs) and sublimation temperatures. Furthermore, the experiment with a partially labeled ^{18}O ice mixture ($C^{18}O-CH_3CH_2OH$) provided mechanistic information and revealed that the ethylene oxide was produced from ethanol. These findings advance our fundamental understanding of the formation mechanisms of oxygen-containing cyclic molecules such as ethylene oxide and their isomers in ethanol-containing interstellar ices through GCR-induced nonequilibrium chemistries, eventually providing valuable insights into the astrochemical evolution of the ISM.

2. Experimental

The experiments were carried out in a stainless steel ultrahigh vacuum chamber evacuated to a base pressure of a few 10^{-11} Torr using magnetically levitated turbomolecular pumps and a dry scroll backing pump (B. M. Jones & R. I. Kaiser 2013). A polished silver substrate was mounted to an oxygen-free, high-conductivity copper target within the main chamber and cooled to low temperatures of 5 K using a two-stage closed-cycle helium cryostat (Sumitomo Heavy Industries, RDK-415E). The cold head was capable of free rotation and vertical translation via a doubly differentially pumped rotational feedthrough and an adjustable bellows. The

experimental procedures have been described in detail previously (J. Wang et al. 2024d). The ethanol (CH_3CH_2OH ; Pharmco, $\geq 99.5\%$ purity) sample was degassed in a borosilicate vial by subjecting it to multiple freeze–thaw cycles with liquid nitrogen so as to remove the residual atmospheric gases. After cooling the substrate to 5 K, the ice mixtures were prepared by depositing premixed gas and vapor with a 2:1 ratio of carbon monoxide (CO; Sigma Aldrich, $>99\%$) to ethanol onto the substrate at a pressure of 4×10^{-8} Torr via a glass capillary array for 18 minutes. Although 5 K is slightly lower than the typical temperature of cold molecular clouds, reactive intermediates can remain intact at this temperature, thus providing valuable mechanistic insights into the experimental results (J. Wang et al. 2024d). During the deposition, the ice growth was monitored via laser interferometry by reflecting a helium-neon laser operating at 632.8 nm off the substrate to a photodiode (A. M. Turner et al. 2015). Using refractive indexes of 1.25 ± 0.03 for CO ice (M. Bouilloud et al. 2015) and 1.26 for CH_3CH_2OH ice (R. L. Hudson 2017), an average index of 1.26 ± 0.04 was determined for carbon monoxide–ethanol ices. The thickness of 880 ± 50 nm was extracted for the $CO-CH_3CH_2OH$ ice. Fourier transform infrared (FTIR) spectra of the deposited ices were collected over a range of $6000-500$ cm^{-1} at a resolution of 4 cm^{-1} using a Nicolet 6700 FTIR spectrometer (Thermo Electron). The ratio of CO to CH_3CH_2OH in the ice mixture was estimated to be (2.5 ± 0.4) :1 (J. Wang et al. 2024d) using the absorption bands of pure CH_3CH_2OH ice with measured thickness and the integrated infrared absorptions of CO at 4249 cm^{-1} ($2\nu_1$, 1.04×10^{-19} cm molecule $^{-1}$) and ^{13}CO at 2091 cm^{-1} (ν_1 , 1.32×10^{-17} cm molecule $^{-1}$) (M. Bouilloud et al. 2015). Note that the absorption coefficients of CO obtained by transmission absorption mode may differ from those measured via reflection absorption mode (S. Ioppolo et al. 2013; D. Qasim et al. 2018). The densities of 0.80 ± 0.01 g cm^{-3} and 0.584 g cm^{-3} were used for CO ice (M. Bouilloud et al. 2015) and CH_3CH_2OH ice (R. L. Hudson 2017), respectively. Density variations for isotopically labeled ice mixtures were accounted for based on the molecular masses of the reactants (J. Wang et al. 2024d). It should be noted that the ratio of carbon monoxide to ethanol studied here does not reflect their typical abundances in molecular clouds; this ratio maximizes the yield of C_2H_4O isomers in the experiments.

After the deposition, the ices were irradiated with 5 keV electrons emitted from an electron gun (SPECS, EQ PU-22) at a current of 23 ± 1 nA for 5 minutes. The electron beam was monitored by a phosphor screen to ensure uniform exposure across the substrate before processing and was then scanned at a 70° angle of incidence over an area of 1.6 cm^2 . The electron current was measured before and after irradiation via a Faraday cup. The irradiation dose was calculated to be 0.14 ± 0.03 eV molecule $^{-1}$ for CO and 0.31 ± 0.05 eV molecule $^{-1}$ for CH_3CH_2OH according to the Monte Carlo simulations using the CASINO 2.42 software suite (D. Drouin et al. 2007); these doses simulate the effects of secondary electrons produced by GCRs in cold molecular clouds aged $(7 \pm 2) \times 10^5$ yr (A. G. Yeghikyan 2011). The average electron penetration depth was calculated to be 420 ± 70 nm for $CO-CH_3CH_2OH$ ice; 99% of the electron energy was deposited within the top 710 ± 50 nm of the ice, which was less than the deposited ice thickness of 880 ± 50 nm, thereby avoiding the interaction between the electrons and the silver substrate. The infrared

spectra of the ice mixtures were collected in situ before, during, and after irradiation. After irradiation, the ice was heated to 320 K at 1 K minute⁻¹ (TPD).

Pulsed (30 Hz) VUV light was used to photoionize the subliming molecules in the gas phase during TPD. Four VUV photon energies were generated through resonant four-wave mixing schemes ($\omega_{\text{VUV}} = 2\omega_1 \pm \omega_2$) using krypton (10.23 eV and 9.71 eV) or xenon (11.10 eV and 9.29 eV) as a nonlinear medium. The laser beams (ω_1 , ω_2) were produced from two tunable dye lasers (Sirah Lasertechnik, Cobra-Stretch) and two neodymium-doped yttrium aluminum garnet (Nd:YAG) lasers (Spectra-Physics, Quanta Ray PRO 250–30 and 270–30). A sum frequency generation scheme ($2\omega_1 + \omega_2$) was used to produce 11.10 eV photons with the 249.628 nm (ω_1) generated by a dye laser and the fundamental (1064 nm; ω_2) of an Nd:YAG laser (J. Wang et al. 2024b). Difference frequency generation schemes ($2\omega_1 - \omega_2$) were employed to produce VUV photons at 10.23 eV and 9.71 eV with 212.556 nm (ω_1) and a dye laser operating at 863.381 or 633.856 nm (ω_2), respectively. The 9.29 eV photons were produced by the difference frequency generation with 222.566 nm (ω_1) and 669.715 nm (ω_2).

A biconvex lithium fluoride lens (Korth Kristalle, $\phi = 38$ mm, $R = 131$ mm) was used in an off-axis geometry to spatially separate VUV light from other laser beams, which was directed 2.0 ± 0.5 mm above the ice surface to photoionize the subliming molecules during TPD. The resulting ions were mass analyzed with reflectron time-of-flight mass spectrometry (ReToF-MS) coupled with a dual microchannel plate (MCP) detector (Jordan TOF Products, Inc.). A preamplifier (Ortec, 9305) amplified the ion signals, which were then discriminated and recorded with a multichannel scaler (FAST ComTec, MCS6A). Each recorded spectrum was the summation of 3600 sweeps (2 minutes) with 3.2 ns bin widths. At 11.10 eV, a blank experiment of CO–CH₃CH₂OH ice was performed without electron irradiation. To confirm the formation mechanisms and mass assignments, experiments with irradiated isotopically labeled ice mixtures were performed using carbon monoxide-¹³C (Sigma Aldrich, ≥ 99 atom % ¹³C), carbon monoxide-¹⁸O (Sigma Aldrich, 95 atom % ¹⁸O), ethanol-d₆ (Cambridge Isotope Laboratories, 99% atom D), and ethanol-¹³C₂ (Sigma Aldrich, 99 atom % ¹³C).

3. Results and Discussion

3.1. FTIR Analysis

FTIR spectra of carbon monoxide–ethanol ices were collected at 5 K before, during, and after electron irradiation at a current of 23 ± 1 nA for 5 minutes. Following irradiation, several new absorptions appeared in the CO–CH₃CH₂OH ice and its isotopically labeled ice mixtures (Figure 2). These absorption features were deconvoluted using Gaussian functions. The asymmetric stretching (ν_3) mode of carbon dioxide was detected at 2342 (CO₂) and 2276 (¹³CO₂) cm⁻¹. The formyl (HCO, ν_3) and *trans*-hydroxycarbonyl (HOCHO, ν_2) radicals were identified by absorptions at 1853 and 1843 cm⁻¹ in irradiated CO–CH₃CH₂OH ice (D. E. Milligan & M. E. Jacox 1964; A. K. Eckhardt et al. 2019) with corresponding shifts observed in irradiated isotopically labeled ice mixtures (Figures 2(b)–(d); A. K. Eckhardt et al. 2019; J. Wang et al. 2023a; J. Wang et al. 2024d). The absorption at 1726 cm⁻¹ in irradiated CO–CH₃CH₂OH ice can be assigned

to the C=O stretching (ν_2) mode of formaldehyde (H₂CO; M. Bouilloud et al. 2015), which shifts respectively to 1695 and 1688 cm⁻¹ in irradiated CO–CD₃CD₂OD ice and ¹³CO–¹³CH₃¹³CH₂OH ice (J. Wang et al. 2024d). A carbonyl functional group, most likely of acetaldehyde, was identified via the C=O stretching (ν_4) mode at 1713 cm⁻¹ for CH₃CHO in irradiated CO–CH₃CH₂OH ice, 1715 cm⁻¹ for CD₃CDO in CO–CD₃CD₂OD ice, and 1675 cm⁻¹ for ¹³CH₃¹³CHO in ¹³CO–¹³CH₃¹³CH₂OH ice (J. Wang et al. 2023a, 2023b). Notably, ethylene oxide exhibits strong absorptions at 1270 and 868 cm⁻¹, attributed to its ring stretch and deformation bands (C. J. Bennett et al. 2005b; R. L. Hudson et al. 2023), while the C=C stretch of vinyl alcohol (CH₂CHOH) has been detected at 1639 cm⁻¹ (C. J. Bennett et al. 2005b). However, these absorptions were not observed due to the low irradiation dose used in the experiments and overlapping absorption features with ethanol, highlighting the need for an alternative experimental technique to identify all individual C₂H₄O isomers.

3.2. PI-ReToF-MS Analysis

The identification of individual C₂H₄O isomers was achieved utilizing PI-ReToF-MS and isotopic substitution experiments during TPD of the irradiated ices. PI-ReToF-MS allows the identification of individual isomers specifically based on differences in their adiabatic IEs and desorption temperature profiles (A. M. Turner & R. I. Kaiser 2020). VUV photons with energies of 11.10, 10.23, 9.71, and 9.29 eV were employed to photoionize the subliming products from processed carbon monoxide–ethanol ices (J. Wang et al. 2024d). The TPD profile of the ion signal at a mass-to-charge (m/z) of 44 for CO–CH₃CH₂OH ice revealed four sublimation events peaking at 107 (peak I), 118 (peak II), 157 (peak III), and 200 K (peak IV) after deconvolution using split Pearson VII distributions (Figure 3(a)). To confirm the molecular formula of the ion signal, separate irradiation experiments with isotopically labeled precursors were conducted. The TPD profile of $m/z = 48$ from fully deuterated ice (CO–CD₃CD₂OD) matches well with that of $m/z = 44$ in CO–CH₃CH₂OH ice (Figure 3(b)), indicating the presence of four hydrogen atoms. Additionally, the TPD profile of $m/z = 44$ in irradiated CO–CH₃CH₂OH ice shifted to $m/z = 46$ in fully ¹³C-labeled ice (¹³CO–¹³CH₃¹³CH₂OH), demonstrating the presence of two carbon atoms (Figure 3(c)). Therefore, the sublimation events of $m/z = 44$ from CO–CH₃CH₂OH ice can be clearly assigned to molecules with the formula C₂H₄O.

As mentioned above, the TPD profile of $m/z = 44$ (C₂H₄O⁺) in irradiated CO–CH₃CH₂OH ice reveals sublimation events labeled as peaks I–IV recorded at 11.10 eV. A blank experiment of the CO–CH₃CH₂OH ice was performed without electron irradiation under otherwise identical conditions, displaying a very small sublimation event peaking at 157 K (Figure 4(a)); this is likely due to impurities in the samples. At 11.10 eV, all C₂H₄O isomers can be photoionized (Figure 1(a)); therefore, peaks I–IV can be associated with any C₂H₄O isomers. Lowering the photon energy to 10.23 eV, at which ethylene oxide (IE = 10.56 ± 0.01 eV; S. G. Lias 2024) cannot be ionized, results in the disappearance of peak IV, while peaks I–III remain (Figure 4(b)), indicating that peak IV is attributable only to ethylene oxide. Thereafter, the photon energy was reduced further to 9.71 eV, at which energy vinyl alcohol (IE = 9.30 ± 0.05 eV (syn); IE = 9.17 ± 0.05 eV

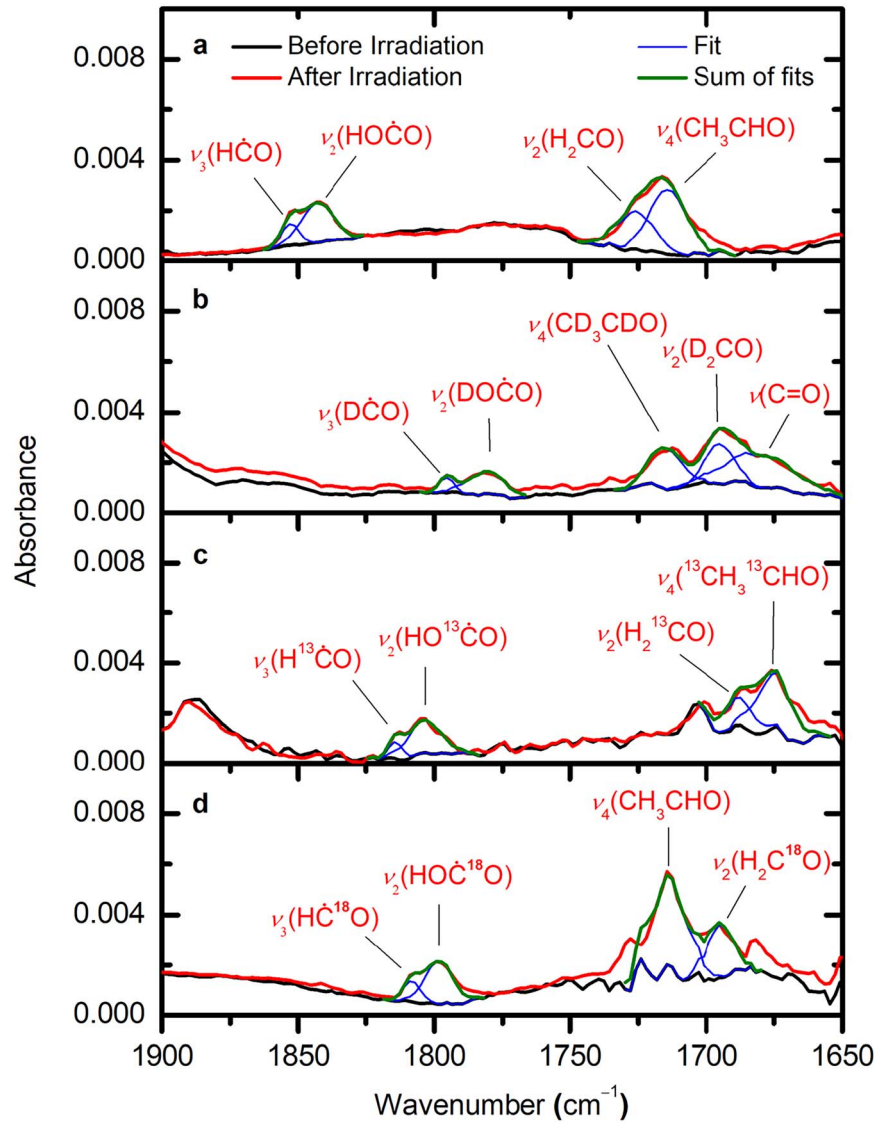


Figure 2. FTIR spectra of carbon monoxide–ethanol ices in the region 1900–1650 cm^{-1} before and after irradiation at 5 K. New absorptions and their corresponding fits are shown for irradiated (a) CO–CH₃CH₂OH ice, (b) CO–CD₃CD₂OD ice, (c) ¹³CO–¹³CH₃¹³CH₂OH ice, and (d) C¹⁸O–CH₃CH₂OH ice.

(anti); G. Y. Matti et al. 1989) can be ionized but not acetaldehyde (IE = 10.2290 ± 0.0007 eV) (S. G. Lias 2024); peak I at 107 K and peak II at 118 K vanish, while peak III at 157 K remains (Figure 4(c)). Therefore, peaks I and II are assigned to acetaldehyde, and peak III can be assigned to vinyl alcohol. Previous studies of electron-irradiated CO–CH₄ ice revealed that acetaldehyde and vinyl alcohol exhibit sublimation events peaking at 117 K and 147 K, respectively (M. J. Abplanalp et al. 2016). It is worth noting that the respective peak sublimation temperatures of ketene (CH₂CO) and ethanol are at 103 K (J. Wang et al. 2023a) and 149 K (J. Wang et al. 2024d), suggesting that peaks I and III may result from cosublimation with ketene and ethanol or are at least perturbed by the simultaneous sublimation of their containing matrix of ice. Further lowering the photon energy to 9.29 eV, which is close to the IEs of vinyl alcohol (IE = 9.30 ± 0.05 eV (syn); IE = 9.17 ± 0.05 eV (anti)), significantly reduces the intensity of peak III (Figure 4(d)), further confirming the association of peak III with vinyl alcohol. An additional experiment with processed C¹⁸O–CH₃CH₂OH ice was conducted. The TPD profile of $m/z = 44$ in

C¹⁸O–CH₃CH₂OH ice matches well with that of $m/z = 44$ in CO–CH₃CH₂OH ice (Figure 3(d)); however, the TPD profile of $m/z = 46$ shows no evidence of peak IV (Figure 5), indicating that ethylene oxide is formed from ethanol alone. In addition, the TPD profile of $m/z = 46$ (C₂H₄¹⁸O⁺) shows small intensities of peaks I and II, indicating that C¹⁸O is the minor contributor ($12 \pm 1\%$) for the formation of acetaldehyde. Overall, the PI-ReToF-MS studies demonstrate the gas-phase detection of all three C₂H₄O isomers.

3.3. Formation Pathways

Having provided compelling evidence on the formation of ethylene oxide and its isomers acetaldehyde and vinyl alcohol in ethanol-containing ices under astrophysical conditions, we now turn our attention to their possible formation pathways. In this study, low-dose irradiation experiments were designed to minimize sequential reactions, thus limiting the possible formation pathways of C₂H₄O isomers. Carbon monoxide is a major component of interstellar ices, making the carbon monoxide–ethanol ice mixture a suitable model ice to investigate the

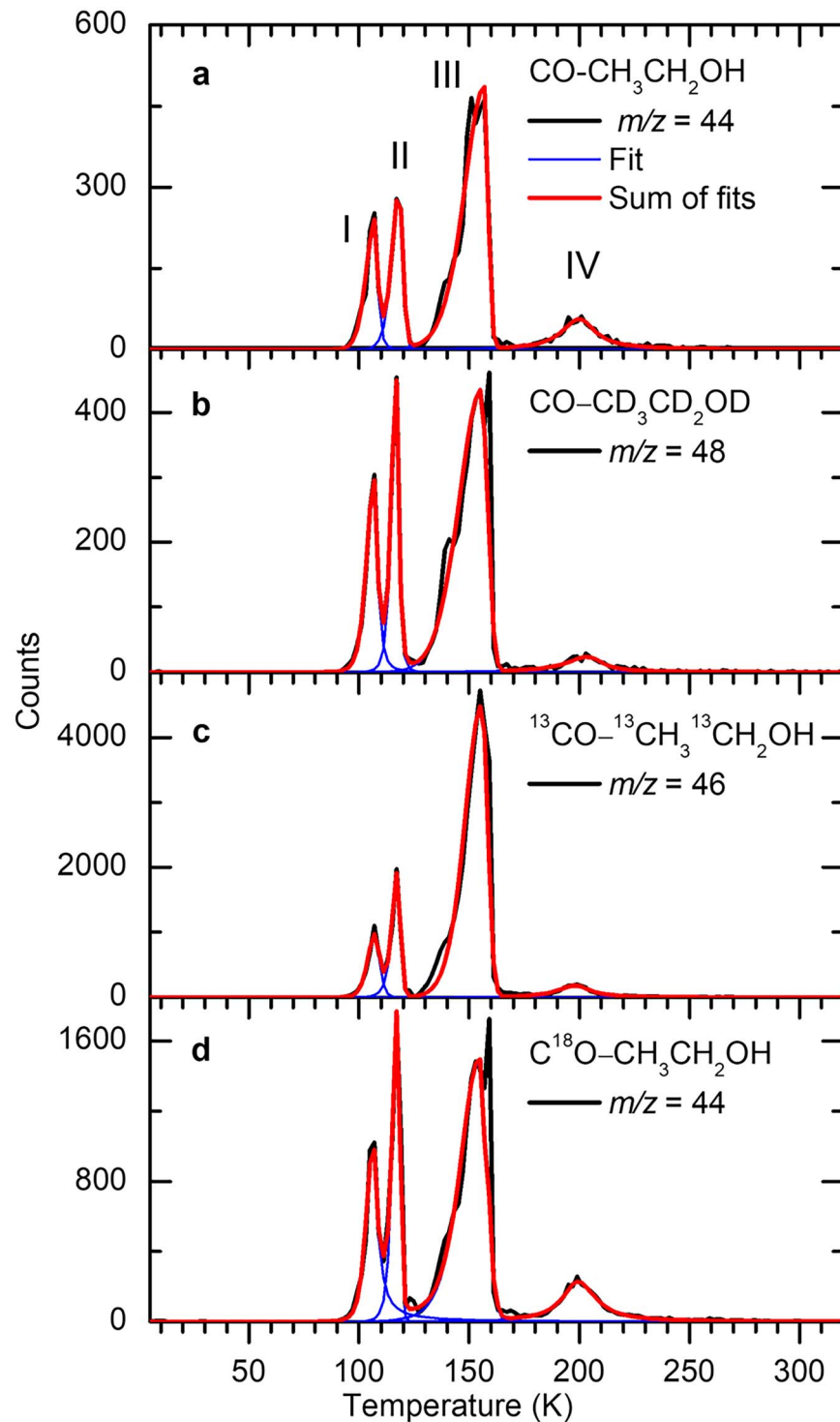


Figure 3. TPD profiles recorded at 11.10 eV for irradiated carbon monoxide–ethanol ice mixtures: (a) $m/z = 44$ in CO–CH₃CH₂OH ice, (b) $m/z = 48$ in CO–CD₃CD₂OD ice, (c) $m/z = 46$ in ¹³CO–¹³CH₃¹³CH₂OH ice, and (d) $m/z = 44$ in C¹⁸O–CH₃CH₂OH ice. The red line indicates the overall fit of each TPD profile.

formation of C₂H₄O isomers. The presence of carbon monoxide contributes to the matrix isolation of reactive intermediates. Additionally, carbon monoxide reacts with atomic hydrogen ($\dot{\text{H}}$) to form formaldehyde and methanol through hydrogenation reactions in low-temperature ices, reducing the availability of atomic hydrogen in the ices. This may promote the stabilization of ethanol radicals, thereby enhancing the formation of C₂H₄O isomers. The unimolecular decomposition of ethanol forms atomic

hydrogen plus ethoxy (CH₃CH₂ $\dot{\text{O}}$), 1-hydroxyethyl (CH₃ $\dot{\text{C}}$ HOH), and 2-hydroxyethyl ($\dot{\text{C}}$ H₂CH₂OH) radicals through endoergic reactions (Reactions (1)–(3); D. Skouteris et al. 2018; P. V. Zasimov et al. 2023; P. V. Zasimov et al. 2024); these reactions are endoergic by 437, 390, and 422 kJ mol⁻¹, respectively (B. Ruscic & H. Bross 2021; A. E. Williams et al. 2021; J. Wang et al. 2024d). During irradiation, the energetic electrons interact with the molecules in the ice and provide sufficient energy

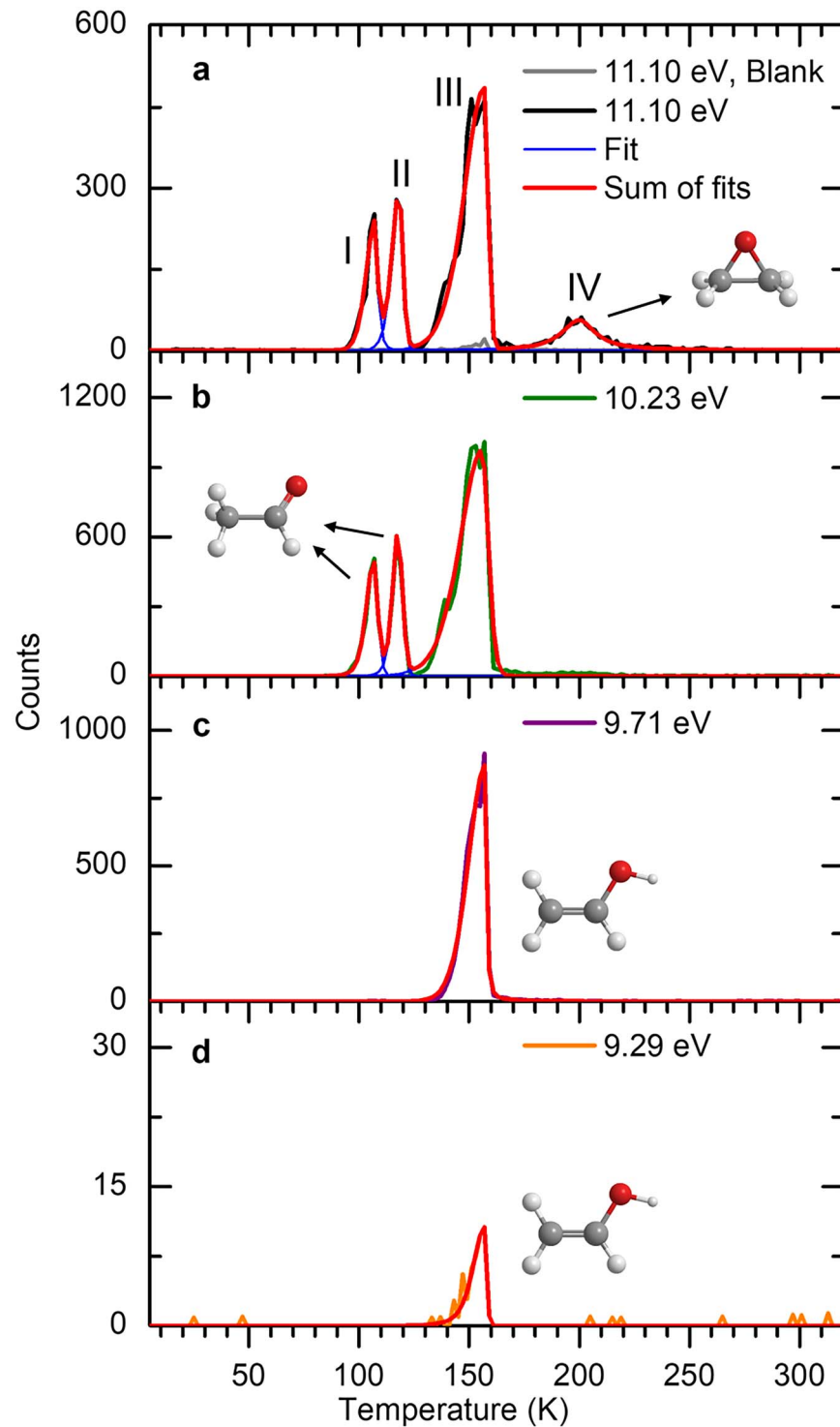
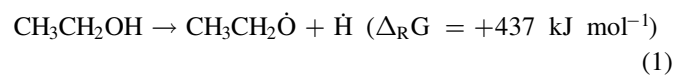


Figure 4. TPD profiles for $m/z = 44$ ($\text{C}_2\text{H}_4\text{O}^+$) in irradiated $\text{CO}-\text{CH}_3\text{CH}_2\text{OH}$ ice recorded at (a) 11.10 eV, (b) 10.23 eV, (c) 9.71 eV, and (d) 9.29 eV, along with the unirradiated (blank) experiment at 11.10 eV (a). The red lines represent the overall fits of the spectra.

to overcome the dissociation barriers. The electrons simulate secondary electrons produced by GCRs penetrating ices in cold molecular clouds. These particles transfer their kinetic energy predominantly to molecules in the ice through inelastic collisions (electronic stopping), which generate secondary electrons that selectively cleave bonds such as C–H and O–H, leading to the production of reactive radicals and ions (R. I. Kaiser et al. 1997; R. I. Kaiser & K. Roessler 1997, 1998; C. N. Shingledecker &

E. Herbst 2018; C. N. Shingledecker et al. 2018). Once formed through ionizing radiation, these radicals can be preserved within the ice mixture due to their limited molecular mobility at low temperatures of 5 K (J. Wang et al. 2024d) and can serve as precursors to the formation of $\text{C}_2\text{H}_4\text{O}$ isomers:



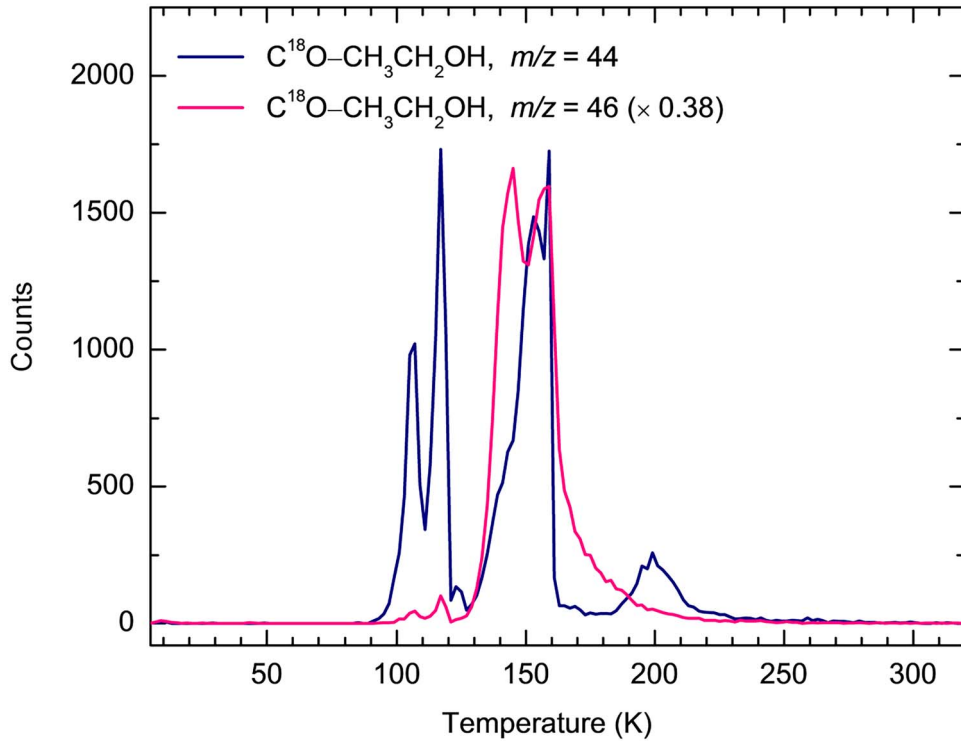
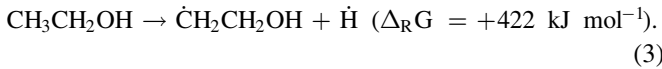
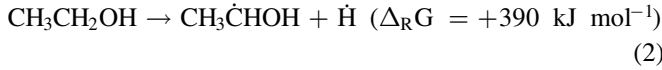
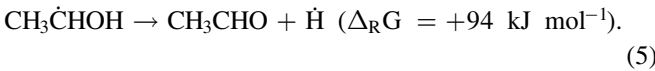
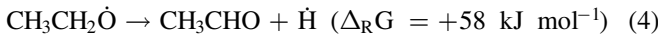


Figure 5. TPD profiles for $m/z = 44$ ($\text{C}_2\text{H}_4\text{O}^+$) and $m/z = 46$ ($\text{C}_2\text{H}_6\text{O}^+$) in irradiated $\text{C}^{18}\text{O}-\text{CH}_3\text{CH}_2\text{OH}$ ice recorded at 11.10 eV.

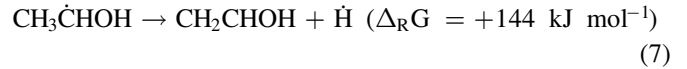
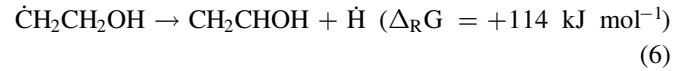


First, acetaldehyde can form from the ethoxy radical (Reaction (4)) and the anti-1-hydroxyethyl radical (Reaction (5)) via C–H bond dissociation. Reactions (4) and (5) are endoergic by 58 kJ mol^{-1} and 94 kJ mol^{-1} , respectively, with reaction barriers of 88 kJ mol^{-1} and 141 kJ mol^{-1} computed at the CCSD(T)/6-311+G(3df, 2p)//B3LYP/6-311+G(3df, 2p) level of theory (Z. F. Xu et al. 2009). Recall that carbon monoxide is the minor contributor leading to acetaldehyde, which could proceed via the barrierless recombination of methyl ($\dot{\text{C}}\text{H}_3$) radical and formyl ($\dot{\text{H}}\text{CO}$) radical (C. J. Bennett et al. 2005a):



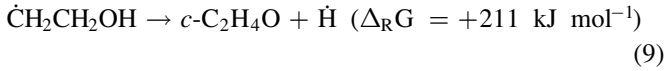
Second, vinyl alcohol can be produced from the *gauche*-2-hydroxyethyl radicals and the *anti*-1-hydroxyethyl radical via Reactions (6) and (7), respectively, which are endoergic by 114 kJ mol^{-1} and 144 kJ mol^{-1} with reaction barriers of 144 kJ mol^{-1} and 164 kJ mol^{-1} computed at the CCSD(T)/6-311+G(d,p)//B3LYP/6-311G(d,p) level of theory (X.-B. Zhang et al. 2002). Vinyl alcohol exists in two conformers, with the hydroxyl group oriented either the same (*syn*-) or opposite (*anti*-) to the carbon–carbon double bond. The *syn*-conformer is calculated to be 5 kJ mol^{-1} lower in energy than the *anti*-conformer (M.-A. Martin-Drumel et al. 2019) and can internally rotate to the *anti*-conformer via a barrier of 17 kJ mol^{-1} (X. Wang et al. 2023c). Additionally,

acetaldehyde can tautomerize to vinyl alcohol through hydrogen migration with an endoergicity of 41 kJ mol^{-1} (Reaction (8)). This reaction pathway has been demonstrated previously in electron-irradiated acetaldehyde ice (N. F. Kleimeier & R. I. Kaiser 2021) and carbon monoxide–methane ice (M. J. Abplanalp et al. 2016). The barrier for keto-enol tautomerization leading to *syn*-vinyl alcohol is 279 kJ mol^{-1} calculated at the CCSD(T)/CBS//B2PLYP-D3(BJ)/ma-def2-TZVP level of theory (X. Wang et al. 2023c):



Third, ethylene oxide can be formed from the 2-hydroxyethyl radical through the loss of an atomic hydrogen (Reaction (9)). The barrier of Reaction (9) leading to ethylene oxide is calculated to be 279 kJ mol^{-1} (N. H. Thọ et al. 2010). Alternatively, ethylene oxide can form via isomerization of acetaldehyde and vinyl alcohol through Reactions (10) and (11), which are endoergic by 116 and 75 kJ mol^{-1} , respectively. Acetaldehyde undergoes an intramolecular hydrogen shift to form a biradical intermediate $\dot{\text{C}}\text{H}_2\text{CH}_2\dot{\text{O}}$ via a barrier of 326 kJ mol^{-1} computed at the CCSD(T)/CBS//B2PLYP-D3(BJ)/ma-def2-TZVP level of theory (X. Wang et al. 2023c), followed by ring closure to produce ethylene oxide (Reaction (10)). Reaction (11) involves two transition states and an intermediate and has the highest reaction barrier of 338 kJ mol^{-1} (X. Wang et al. 2023c). The barriers to these reaction pathways can be overcome by the energy contributed

by GCRs proxies (J. Wang et al. 2022):



4. Astrophysical Implications and Conclusions

This study presents the first laboratory simulation experiments on the formation of three astronomically observed $\text{C}_2\text{H}_4\text{O}$ isomers—ethylene oxide ($c\text{-C}_2\text{H}_4\text{O}$), acetaldehyde (CH_3CHO), and vinyl alcohol (CH_2CHOH)—in model interstellar ices composed of carbon monoxide and ethanol. The ice mixtures were exposed to energetic electrons that act as proxies for GCR irradiation within cold molecular clouds, with irradiation doses as low as $0.14 \pm 0.03 \text{ eV molecule}^{-1}$ for carbon monoxide and $0.31 \pm 0.05 \text{ eV molecule}^{-1}$ for ethanol. These doses correspond to $(7 \pm 2) \times 10^5 \text{ yr}$, equivalent to the early stage of a molecular cloud, which typically has a lifetime of up to $5 \times 10^7 \text{ yr}$ (A. G. Yeghikyan 2011). It should be noted that no simulation experiment can replicate the complexity of the interstellar environment; however, laboratory simulation experiments conducted with well-defined irradiation doses help understand the reaction pathways leading to key organics such as oxygen-containing cyclic molecules in the ices. Ethylene oxide, acetaldehyde, and vinyl alcohol were detected in the gas phase using PI-ReToF-MS during TPD, which simulates the heating that results from the transition of a cold molecular cloud to star formation. Our findings reveal feasible pathways for the formation of $\text{C}_2\text{H}_4\text{O}$ isomers in ethanol-containing ices, providing valuable constraints on astrochemical modeling for their formation in extraterrestrial environments. Future experiments could investigate the formation of these isomers by incorporating water—the most abundant molecule in interstellar ices (K. I. Öberg et al. 2011)—into the ice mixture; The $\text{C}_2\text{H}_6\text{O}_2$ isomers such as ethylene glycol ($\text{HOCH}_2\text{CH}_2\text{OH}$) may be formed in electron-irradiated ethanol–water ice.

Ethylene oxide and acetaldehyde have been observed toward multiple sources including Sgr B2N, NGC 6334 F, G327.3–0.6, and G31.41+0.31 (N. Fourikis et al. 1974; M. B. Bell et al. 1983; J. E. Dickens et al. 1997; A. Nummelin et al. 1998; M. Ikeda et al. 2001). Ethylene oxide has been proposed as a potential contributor to some unidentified infrared emission features (L. S. Bernstein & D. K. Lynch 2009). Vinyl alcohol has also been identified toward Sgr B2N (B. E. Turner & A. J. Apponi 2001), which remains the only interstellar environment where all $\text{C}_2\text{H}_4\text{O}$ isomers have been detected. Since gas-phase reaction schemes alone cannot account for their observed abundances (M. Ikeda et al. 2001), these molecules are believed to form in interstellar ices via ionizing radiation sources such as protons (R. L. Hudson & M. H. Moore 2003), electrons (C. J. Bennett et al. 2005a; C. J. Bennett et al. 2005b), and photons (K. M. Yocum et al. 2021). A gas-grain chemical model has reproduced the abundances of ethylene oxide and acetaldehyde in high-mass star-forming regions (A. Occhiogrosso et al. 2014). Notably, ethanol has also been detected toward Sgr B2N with a column density of up to $9.1 \times 10^{17} \text{ cm}^{-2}$ (A. Belloche et al. 2013; B. Zuckerman et al. 1975). Therefore, our results suggest that ethanol may contribute to the astronomical observations of $\text{C}_2\text{H}_4\text{O}$ isomers in Sgr B2N. Furthermore, an isotopic labeling

experiment using $\text{C}^{18}\text{O}\text{-CH}_3\text{CH}_2\text{OH}$ ice demonstrated that ethylene oxide is produced from ethanol alone, providing the first experimental evidence supporting the hypothesis that ethanol can serve as a precursor to ethylene oxide in interstellar ices (M. Ikeda et al. 2001; A. Occhiogrosso et al. 2012; D. Skouteris et al. 2018).

Ethanol is ubiquitous in the ISM and has also been identified toward star-forming regions such as Orion-KL (N. Brouillet et al. 2013) and W51M (T. J. Millar et al. 1988), as well as hot-core regions including NGC 6334 IRS1, NGC 7538 IRS1, and W3(H₂O) (S. E. Bisschop et al. 2007). It has also been detected toward the molecular cloud associated with the ultracompact H II region G34.3+0.15 (T. J. Millar et al. 1995). Laboratory simulation experiments have shown that ethanol can be effectively formed in electron-irradiated methane–water ice and methane–methanol ice via radical-radical recombination reactions (A. Bergantini et al. 2017; A. Bergantini et al. 2018b). Recent studies have tentatively identified ethanol in ices toward background stars such as NIR38 and J110621 (M. K. McClure et al. 2023) and young protostars like the IRAS 2 A and IRAS 23385, with abundances as high as 1.8% relative to water (W. R. M. Rocha et al. 2024). Following the reaction pathways as proposed in this study, $\text{C}_2\text{H}_4\text{O}$ isomers can form in ethanol-containing interstellar ices within cold molecular clouds and may act as precursors to key prebiotic molecules. For instance, acetaldehyde can serve as a key precursor to molecules relevant to astrobiology such as pyruvic acid (CH_3COCO); N. F. Kleimeier et al. 2020b). Ethylene oxide may react with methane and hydrogen cyanide (HCN) to form chiral propylene oxide and oxirane-2-carbonitrile ($c\text{-C}_3\text{H}_3\text{NO}$), respectively. Oxirane-2-carbonitrile has been searched for in cold, quiescent, and hot-core type interstellar molecular clouds, with an upper limit of 10^{-10} relative to molecular hydrogen (J. E. Dickens et al. 1996). Once formed in interstellar ices in a cold molecular cloud, these organics can eventually sublime into the gas phase as the molecular cloud transitions to the hot-core stage, representing promising candidates for astronomical searches via telescopes such as the James Webb Space Telescope the Atacama Large Millimeter/submillimeter Array. Furthermore, these compounds could be delivered to planets like the early Earth via meteoritic parent bodies, constituting an exogenous source of biorelevant molecules (C. Chyba & C. Sagan 1992; A. Shimoyama & R. Ogasawara 2002). In fact, extraterrestrial aldehydes including acetaldehyde have been detected in carbonaceous chondrites (J. C. Aponte et al. 2019) and comets such as 67 P/Churyumov-Gerasimenko (M. Schuhmann et al. 2019).

Lastly, our results represent a critical step toward the systematic elucidation of the formation mechanisms of oxygen-containing cyclic molecules, aldehydes, and their enol tautomers in alcohol-containing interstellar ices. For example, propylene oxide and propanal ($\text{CH}_3\text{CH}_2\text{CHO}$), detected in Sgr B2N (J. M. Hollis et al. 2004; B. A. McGuire et al. 2016), may form in interstellar ices containing *n*-propanol ($\text{CH}_3\text{CH}_2\text{CH}_2\text{OH}$) and/or *i*-propanol ($\text{CH}_3\text{CH}(\text{OH})\text{CH}_2$), which have been recently identified toward Sgr B2N as well (A. Belloche et al. 2022). Additionally, ethylene glycol ($\text{HOCH}_2\text{CH}_2\text{OH}$) can serve as a precursor to the glycolaldehyde (HCOCH_2OH) enol 1,2-ethenediol (HOCH-CHOH ; N. F. Kleimeier et al. 2021b), which has been observed toward the G+0.693–0.027 molecular cloud located in the Galactic center (V. M. Rivilla et al. 2022). These reaction pathways could occur via GCR-induced nonequilibrium

chemistries in alcohol-containing ices, advancing our fundamental understanding of the formation mechanisms of oxygen-containing COMs in deep space.

Acknowledgments

We acknowledge support from the U.S. National Science Foundation (NSF), Division of Astronomical Sciences (AST-2403867), awarded to the University of Hawaii at Manoa (R.I.K.). We also thank the W. M. Keck Foundation and the University of Hawaii at Manoa for their support in constructing the experimental setup.

ORCID iDs

Jia Wang  <https://orcid.org/0000-0002-3795-8699>
 Chaojiang Zhang  <https://orcid.org/0000-0003-3727-901X>
 Joshua H. Marks  <https://orcid.org/0000-0003-0492-2494>
 Ralf I. Kaiser  <https://orcid.org/0000-0002-7233-7206>

References

- Abplanalp, M. J., Gozem, S., Krylov, A. I., et al. 2016, *PNAS*, **113**, 7727
 Aponte, J. C., Whitaker, D., Powner, M. W., Elsila, J. E., & Dworkin, J. P. 2019, *ESC*, **3**, 463
 Ball, J. A., Gottlieb, C. A., Lilley, A. E., & Radford, H. E. 1970, *ApJ*, **162**, L203
 Barone, V., Biczysko, M., & Pazzarini, C. 2015, *Acc. Chem. Res.*, **48**, 1413
 Bell, M. B., Mathews, H. E., & Feldman, P. A. 1983, *A&A*, **127**, 420
 Belloche, A., Garrod, R. T., Zingsheim, O., Müller, H. S. P., & Menten, K. M. 2022, *A&A*, **662**, A110
 Belloche, A., Müller, H. S. P., Menten, K. M., Schilke, P., & Comito, C. 2013, *A&A*, **559**, A47
 Bennett, C. J., Jamieson, C. S., Osamura, Y., & Kaiser, R. I. 2005a, *ApJ*, **624**, 1097
 Bennett, C. J., Osamura, Y., Lebar, M. D., & Kaiser, R. I. 2005b, *ApJ*, **634**, 698
 Bergantini, A., Abplanalp, M. J., Pokhilko, P., et al. 2018a, *ApJ*, **860**, 108
 Bergantini, A., Góbi, S., Abplanalp, M. J., & Kaiser, R. I. 2018b, *ApJ*, **852**, 70
 Bergantini, A., Maksyutenko, P., & Kaiser, R. I. 2017, *ApJ*, **841**, 96
 Bergner, J. B., Öberg, K. I., & Rajappan, M. 2019, *ApJ*, **874**, 115
 Bernard, J. M., Coll, P., Coustenis, A., & Raulin, F. 2003, *P&SS*, **51**, 1003
 Bernstein, L. S., & Lynch, D. K. 2009, *ApJ*, **704**, 226
 Bhat, B., Kar, R., Mondal, S. K., et al. 2023, *ApJ*, **958**, 111
 Bisschop, S. E., Jørgensen, J. K., van Dishoeck, E. F., & de Wachter, E. B. M. 2007, *A&A*, **465**, 913
 Bouilloud, M., Fray, N., Benilan, Y., et al. 2015, *MNRAS*, **451**, 2145
 Brouillet, N., Despois, D., Baudry, A., et al. 2013, *A&A*, **550**, A46
 Charnley, S. B. 2004, *AdSpR*, **33**, 23
 Chyba, C., & Sagan, C. 1992, *Natur*, **355**, 125
 Cuppen, H. M., Linnartz, H., & Ioppolo, S. 2024, *ARA&A*, **62**, 243
 Dai, Z., Gao, S., Wang, J., & Mo, Y. 2014, *JChPh*, **141**, 144306
 Dickens, J. E., Irvine, W. M., Ohishi, M., et al. 1996, *OLEB*, **26**, 97
 Dickens, J. E., Irvine, W. M., Ohishi, M., et al. 1997, *ApJ*, **489**, 753
 Drouin, D., Couture, A. R., Joly, D., et al. 2007, *J. Scanning Microsc.*, **29**, 92
 Eckhardt, A. K., Bergantini, A., Singh, S. K., Schreiner, P. R., & Kaiser, R. I. 2019, *Angew. Chem.*, **58**, 5663
 Fourikis, N., Sinclair, M., Robinson, B., Godfrey, P., & Brown, R. 1974, *AuJPh*, **27**, 425
 Gibb, E. L., Whittet, D. C. B., Boogert, A. C. A., & Tielens, A. G. G. M. 2004, *ApJS*, **151**, 35
 Herbst, E., & Dishoeck, E. F. V. 2009, *ARA&A*, **47**, 427
 Hollis, J. M., Jewell, P. R., Lovas, F. J., Remijan, A., & Møllendal, H. 2004, *ApJ*, **610**, L21
 Hudson, R. L. 2017, *AcSpA*, **187**, 82
 Hudson, R. L., Gerakines, P. A., & Yarnall, Y. Y. 2023, *Icar*, **396**, 115499
 Hudson, R. L., & Moore, M. H. 2003, *ApJ*, **586**, L107
 Ikeda, M., Ohishi, M., Nummelin, A., et al. 2001, *ApJ*, **560**, 792
 Ioppolo, S., Fedoseev, G., Lamberts, T., Romanzin, C., & Linnartz, H. 2013, *RSci*, **84**, 073112
 Jones, B. M., & Kaiser, R. I. 2013, *JPCL*, **4**, 1965
 Kaiser, R. I., Eich, G., Gabrysch, A., & Roessler, K. 1997, *ApJ*, **484**, 487
 Kaiser, R. I., & Roessler, K. 1997, *ApJ*, **475**, 144
 Kaiser, R. I., & Roessler, K. 1998, *ApJ*, **503**, 959
 Karton, A., & Talbi, D. 2014, *CP*, **436**, 22
 Kleimeier, N. F., Abplanalp, M. J., Johnson, R. N., et al. 2021a, *ApJ*, **911**, 24
 Kleimeier, N. F., Eckhardt, A. K., & Kaiser, R. I. 2020a, *ApJ*, **901**, 84
 Kleimeier, N. F., Eckhardt, A. K., & Kaiser, R. I. 2021b, *J. Am. Chem. Soc.*, **143**, 14009
 Kleimeier, N. F., Eckhardt, A. K., Schreiner, P. R., & Kaiser, R. I. 2020b, *Chem*, **6**, 3385
 Kleimeier, N. F., & Kaiser, R. I. 2021, *ChPhC*, **22**, 1229
 Lias, S. G. 2024, in NIST Chemistry WebBook, NIST Standard Reference Database Number 96, ed. P. J. Linstrom & W. G. Mallard (Gaithersburg, MD: NIST)
 Marks, J. H., Nikolayev, A. A., Evseev, M. M., et al. 2023, *Chem*, **9**, 3286
 Martin-Drumel, M.-A., Lee, K. L. K., Belloche, A., et al. 2019, *A&A*, **623**, A167
 Mathews, H. E., Friberg, P., & Irvine, W. M. 1985, *ApJ*, **290**, 609
 Matti, G. Y., Osman, O. I., Upham, J. E., Suffolk, R. J., & Kroto, H. W. 1989, *JESRP*, **49**, 195
 McClure, M. K., Rocha, W. R. M., Pontoppidan, K. M., et al. 2023, *NatAs*, **7**, 431
 McGuire, B. A., Carroll, P. B., Loomis, R. A., et al. 2016, *Sci*, **352**, 1449
 Millar, T. J., Brown, P. D., Olofsson, H., & Hjalmarsen, A. 1988, *A&A*, **205**, L5
 Millar, T. J., MacDonald, G. H., & Habing, R. J. 1995, *MNRAS*, **273**, 25
 Milligan, D. E., & Jacox, M. E. 1964, *JChPh*, **41**, 3032
 Müller, H. S. P., Jørgensen, J. K., Guillemin, J.-C., Lewen, F., & Schlemmer, S. 2023a, *MNRAS*, **518**, 185
 Müller, H. S. P., Jørgensen, J. K., Guillemin, J.-C., Lewen, F., & Schlemmer, S. 2023b, *JMoSp*, **394**, 111777
 Nummelin, A., Dickens, J. E., Bergman, P., et al. 1998, *A&A*, **337**, 275
 Öberg, K. I., Boogert, A. A., Pontoppidan, K. M., et al. 2011, *ApJ*, **740**, 109
 Occhiogrosso, A., Vasyunin, A., Herbst, E., et al. 2014, *A&A*, **564**, A123
 Occhiogrosso, A., Vitù, S., Ward, M. D., & Price, S. D. 2012, *MNRAS*, **427**, 2450
 Pazzarini, C., Baiardi, A., Bloino, J., et al. 2017, *AJ*, **154**, 82
 Qasim, D., Chuang, K.-J., Fedoseev, G., et al. 2018, *A&A*, **612**, A83
 Rivilla, V. M., Colzi, L., Jiménez-Serra, I., et al. 2022, *ApJL*, **929**, L11
 Rocha, W. R. M., van Dishoeck, E. F., Ressler, M. E., et al. 2024, *A&A*, **683**, A124
 Ruscic, B., & Bross, H. 2021, Active Thermochemical Tables (ATcT) Thermochemical Values, ver. 1.122r, doi:10.17038/CSE/1822363
 Schuhmann, M., Altwegg, K., Balsiger, H., et al. 2019, *ESC*, **3**, 1854
 Sharma, M. K., Sharma, M., & Chandra, S. 2018, *Ap&SS*, **363**, 94
 Shimoyama, A., & Ogasawara, R. 2002, *OLEB*, **32**, 165
 Shingledecker, C. N., & Herbst, E. 2018, *PCCP*, **20**, 5359
 Shingledecker, C. N., Tennis, J., Gal, R. L., & Herbst, E. 2018, *ApJ*, **861**, 20
 Singh, S. K., Fabian Kleimeier, N., Eckhardt, A. K., & Kaiser, R. I. 2022, *ApJ*, **941**, 103
 Singh, S. K., La Jeunesse, J., Zhu, C., et al. 2020a, *Chem. Comm.*, **56**, 15643
 Singh, S. K., Tsai, T.-Y., Sun, B.-J., et al. 2020b, *J. Phys. Chem. Lett.*, **11**, 5383
 Skouteris, D., Balucani, N., Ceccarelli, C., et al. 2018, *ApJ*, **854**, 135
 Thi, W.-F., van Dishoeck, E. F., Dartois, E., et al. 2006, *A&A*, **449**, 251
 Thọ, N. H., Hue, N. M., & Quang, D. T. 2010, *Vietnam J. Chem.*, **48**, 485
 Thripati, S., Gautam, R., & Ramabhadran, R. O. 2023, *ESC*, **3**, 77
 Turner, A. M., Abplanalp, M. J., Chen, S. Y., et al. 2015, *PCCP*, **17**, 27281
 Turner, A. M., & Kaiser, R. I. 2020, *Acc. Chem. Res.*, **53**, 2791
 Turner, B., Terzieva, R., & Herbst, E. 1999, *ApJ*, **518**, 699
 Turner, B. E. 1991, *ApJS*, **76**, 617
 Turner, B. E., & Apponi, A. J. 2001, *ApJ*, **561**, L207
 Wang, J., Marks, J. H., Batrakova, E. A., et al. 2024a, *Phys. Chem. Chem. Phys.*, **26**, 23654
 Wang, J., Marks, J. H., Fortenberry, R. C., & Kaiser, R. I. 2024b, *SciA*, **10**, eadl3236
 Wang, J., Marks, J. H., Tuli, L. B., et al. 2022, *JPCA*, **126**, 9699
 Wang, J., Marks, J. H., Turner, A. M., et al. 2023a, *SciA*, **9**, eadg1134
 Wang, J., Marks, J. H., Turner, A. M., et al. 2023b, *PCCP*, **25**, 936
 Wang, J., Turner, A. M., Marks, J. H., Fortenberry, R. C., & Kaiser, R. I. 2024c, *Chem. Phys. Chem.*, **25**, e202400837
 Wang, J., Zhang, C., Marks, J. H., et al. 2024d, *NatCo*, **15**, 10189
 Wang, X., Ye, L., Zhang, X., et al. 2023c, *CoFl*, **250**, 112634
 Ward, M. D., & Price, S. D. 2011, *ApJ*, **741**, 121
 Williams, A. E., Hammer, N. I., & Tschumper, G. S. 2021, *JChPh*, **155**, 114306
 Woon, D. E. 2025, The Astrochymist (accessed 2025 April 18), <http://www.astrochymist.org/>

- Xu, Z. F., Xu, K., & Lin, M. C. 2009, *Chem. Phys. Chem.*, 10, 972
- Yeghikyan, A. G. 2011, *Ap*, 54, 87
- Yocum, K. M., Milam, S. N., Gerakines, P. A., & Wadlicus Weaver, S. L. 2021, *ApJ*, 913, 61
- Zasimov, P. V., Sanochkina, E. V., Tyurin, D. A., & Feldman, V. I. 2023, *PCCP*, 25, 4624
- Zasimov, P. V., Volosatova, A. D., Góbi, S., et al. 2024, *J. Chem. Phys.*, 160, 024308
- Zhang, X.-B., Liu, J.-J., Li, Z.-S., Liu, J.-Y., & Sun, C.-C. 2002, *JPCA*, 106, 3814
- Ziurys, L. M., & McGonagle, D. 1993, *ApJS*, 89, 155
- Zuckerman, B., Turner, B., Johnson, D., et al. 1975, *ApJ*, 196, L99